Experiments in Fluids (2021) 62:212
https://doi.org/10.1007/s00348-021-03306-4

RESEARCH ARTICLE

FLEET velocimetry measurements in the ONR-UTA arc-jet wind tunnel

Vijay Gopal[1] · Daniel Palmquist[1] · Luca Maddalena[1] · Laura E. Dogariu[2] · Arthur Dogariu[3]

Received: 22 June 2021 / Revised: 1 September 2021 / Accepted: 7 September 2021 / Published online: 30 September 2021

Abstract

This manuscript presents and discusses the very first successful application of the Femtosecond Laser Electronic Excitation Tagging (FLEET) velocimetry technique in an arc-jet flow. Specifically, one-dimensional, quantitative, FLEET velocimetry data were obtained in the effort to characterize the 1.6 MW ONR-UTA arc-jet plasma wind tunnel, *Leste*, housed at the Aerodynamics Research Center of the University of Texas at Arlington. While the FLEET technique has been used in other types of high-speed wind tunnel facilities, application to flows with high background radiation, such as arc-jets, has never been demonstrated before this work. The high background emissions posed concerns on the feasibility of performing FLEET velocimetry measurements. However, this work demonstrates how these concerns were addressed and presents the first successful application of the FLEET technique in arc-jet flows. The FLEET emissions in the arc-jet plume were successfully imaged, and a significant spatio-temporal variation in the tag's displacement was observed. For the selected operational condition in this study, the average measured gas velocity in the arc-jet plume was 1.78 km/s.

Graphic abstract

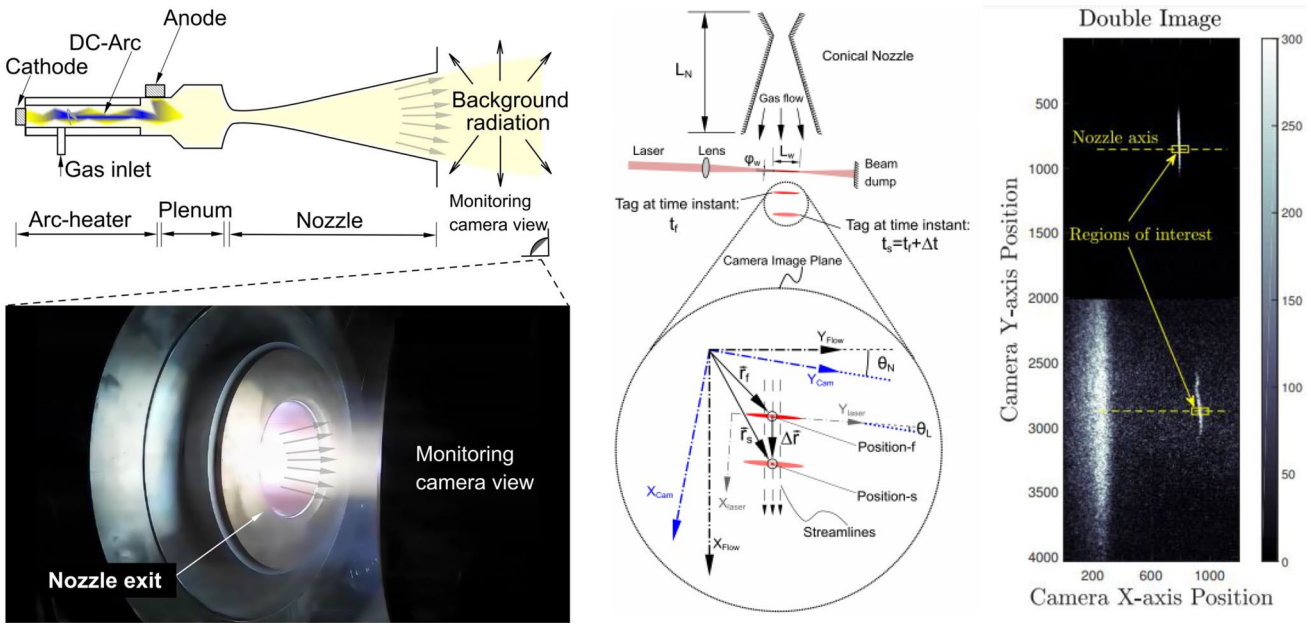

This material is based upon research supported by, or in part by, the U.S. Office of Naval Research under Award Number N00014-19-1-2250. This research used resources of the Princeton Collaborative Low Temperature Plasma Research Facility (PCRF), which is a collaborative research facility supported by the U.S. Department of Energy, Office of Science, Office of Fusion Energy Sciences under Award Number DE-SC0021154.

Extended author information available on the last page of the article

1 Introduction

For more than 60 years, arc-jet testing has served as primary basis for characterizing Thermal Protection Systems (TPS) in support of material development and response

model validation. Arc-jet facilities provide the only ground-based means of simulating hypersonic heating rates (entry, re-entry, hypersonic cruise) in a reacting flow environment under flight-relevant durations. Arc-jet testing provides data for detail material response models that can reduce uncertainty and the magnitude of thickness margins. Arc-jets are also essential to investigate mechanical failure modes including erosion, spallation, and losses related to shear effects. The ability to perform accurate experiments using arc-jet facilities is tightly coupled with the necessity of a careful characterization of the resulting plasma flow. The high uncertainties associated with this class of flows strongly impact the development of new TPS as well as the progress in the fundamental understanding of associated gas-surface interaction phenomena. The flow characterization in representative conditions (including thermo-chemical non-equilibrium), and the use of advanced diagnostic tools to study the chemistry and physics of the boundary layer are of primary importance.

Although arc-jet tests are indicative of how well a material will perform in extreme aerothermal heating environments, it has not been possible to directly relate arc-jet test results to flight applications. The main obstacle has been an inability to determine the total enthalpy of the nonequilibrium arc-jet flow, and its distribution among kinetic, thermal, and chemical modes.

Additionally, due to the difficulty of modeling the complex thermochemistry inside the arc heater, high-fidelity computational fluid dynamics (CFD) efforts are typically restricted to the convergent-divergent nozzle and the test section. The spatial profile of the nozzle inlet conditions is generally modeled neglecting many thermo-physical and fluid dynamics phenomena. Bypassing the complex mixing problem in the plenum and neglecting flow nonuniformities, however, hinders the accuracy of CFD simulations. As a result, reliable measurements of arc-heater conditions are needed to properly anchor and improve the accuracy of the CFD analysis.

Characterizing the complex flow conditions produced in the arc-jet plume requires advanced experimental measurement techniques and computational models. Specifically, the velocity of the gas, $|\mathbf{V}|$, contains important information on the total enthalpy, $h_o = h + |\mathbf{V}|^2/2$, of the flow. Only a few studies in the literature present velocity measurements in arc-jet flows using non-intrusive measurement techniques. Some of the techniques include spectroscopic methods such as the emission Doppler shift technique as shown by Beth and Kling (1969); Scott (1993) and the laser-induced fluorescence Doppler technique by Arepalli (1989). Recent efforts to measure velocity in arc-jet flows include an excitation scanning technique for Doppler shift measurements using nano-second Two-Photon Absorption Laser Induced Fluorescence (ns-TALIF) at the NASA Ames Interaction Heating Facility by Grinstead et al. (2011, 2016) and Nitric Oxide Planar Laser Induced Fluorescence (NO PLIF) measurements in the HYMETS facility at NASA Langley by Inman et al. (2013). Most of these studies in arc-jet flows only measured a single component of the velocity along the mean flow direction using a given measurement technique. State-of-the-art femto-second (fs) laser systems offer accurate measurements of velocity of the gas using the Femtosecond Laser Electronic Excitation Tagging (FLEET) technique (Michael et al. 2011, 2012; Miles 2013; Dogariu et al. 2018a). This velocity measurement technique has two primary advantages. First, it does not require any information on the thermo-physical state of the probed gas, and second, there is no need to introduce tracer particles that may not faithfully follow the flow. The FLEET technique has also been extended to perform three-component velocimetry (Danehy et al. 2014) using an arrangement with a single camera and multiple mirrors. Particularly, measurement of the three components of velocity will be useful in characterizing turbulence in high-speed flows.

The fs-laser utilized in the FLEET technique dissociates diatomic nitrogen molecules in the flow to form atomic nitrogen. The eventual recombination process is associated with near infra-red emissions (or afterglow). These emissions can last for tens of microseconds and thereby providing ample time for detectable displacement of the tagged molecules in the flowing gas. A camera with short time-gated recording capability and a set delay is used for sequential imaging of the tagged emissions. Two successive images recorded by the camera are utilized to calculate the spatial displacement of the tag and retrieve its velocity. Alternate variants of the FLEET technique have been applied in laboratory environments, particularly the Pico-second Laser Electronic Excitation Tagging (PLEET) for high-frequency measurements ($\sim$ 100 KHz, Hsu et al. 2020), and selective two-photon absorptive resonance FLEET (or STARFLEET) technique utilizes an ultraviolet nitrogen dissociative state at 202.25 nm resonance to reduce the energy required to dissociate the molecular nitrogen. The tag generated in this technique is associated with a small temperature rise ($\sim$ 10 K) in the tag volume (Reese et al. 2018). The tagging process of nitrogen gas flows using FLEET involves focusing a fs-laser that is pulsed at $\lambda_l \sim 800$ nm to achieve a high-energy flux, of the order $\sim 10^{14}$W/cm^2, inside the beam-waist region (DeLuca et al. 2014). The high photon-flux through this region enables photodissociation of the ground state of diatomic nitrogen, $N_2(X^1\Sigma_g^+)$ to form atomic nitrogen, $N(^4S)$, through multi-photon absorption processes and/or tunneling processes (Peters et al. 2019). Higher energetic photons at shorter wavelengths were considered by DeLuca et al. (2014) to investigate a method to ease the process of photodissociation by reducing the number of photons required in a single absorption process; however, the rapid

loss in the pulse energy during the frequency conversion process inside the fs-laser system was found to quickly offsets the gains made at shorter wavelength.

The FLEET technique requires one laser and one camera which simplifies the complexity in the experimental setup that is particularly attractive to apply in complex environments such as high-speed wind tunnel facilities. Recent application of FLEET at AEDC Hypervelocity Wind Tunnel 9 was carried out at Mach 10, 14 and 18 (Dogariu et al. 2018b, 2019, 2021). While the FLEET technique has been used in other types of facilities, application to flows with high background radiation, such as arc-jets, has never been demonstrated before this work. The high background emissions posed concerns on the feasibility of performing FLEET velocimetry measurements. However, this work demonstrates how these concerns were addressed and presents the first successful application of the FLEET technique in arc-jet flows. At the Aerodynamics Research Center (ARC) of the University of Texas at Arlington (UTA), a new 1.6 MW ONR-UTA arc-jet plasma wind tunnel was commissioned in 2019 and was utilized for this research.

2 Overview of the FLEET velocimetry technique and arc-jet flow applications

In this section, a brief overview on FLEET emission process is detailed. Following this, the FLEET velocimetry method that is utilized for arc-jet application is discussed.

2.1 Nitrogen FLEET excitation and emissions

A schematic of the anharmonic potential energy curves for different electronic configurations of diatomic nitrogen is presented in Fig. 1. The dissociation energy for the nitrogen molecule, $N_2(X^1\Sigma_g^+)$, from its ground vibrational energy state is about $D_e \sim 9.8$ eV. In general, the photodissociation process involves formation of a predissociation species at an electronically excited state which eventually transfers from its bounded state (i.e., diatomic configuration N ≡ N) to its unbounded state (mono-atomic configuration, N) resulting in two separate neutral atoms (Heays 2010). To form the predissociation species from the ground vibrational state of the molecule, the energy demand is greater than D_e. However, the formation of monoatomic nitrogen, $N(^4S)$, in the FLEET excitation process is thought to arise from a different mechanism (Peters et al. 2019). As the excitation process in FLEET utilizes a focused infrared laser, it is suggested that the tunneling process more likely results in photoionization of N_2 in the gas forming N_2^+ and e^- rather than forming a predissociation species. The electron-ion recombination process results in the formation of mono-atomic nitrogen $N(^4S)$. The ionization energy requirement for a single nitrogen molecule is $U_{N_2^+} \sim 15.6$ eV. Therefore, if the wavelength of the fs-laser pulse is at ~ 800 nm with each photon carrying energy $h\nu_l \sim 1.5$ eV, then the number of photons absorbed by a single molecule is $\lceil U_{N_2^+}/h\nu_l \rceil = 11$. As a result of the electron-ion recombination process, the dominant species in the beam waist that are relevant to FLEET emissions include diatomic nitrogen in its C-state $N_2(C^3\Pi_u)$, B-state $N_2(B^3\Pi_g)$, A-state, $N_2(A^3\Sigma_u^+)$, B-state ion, $N_2^+(B^2\Sigma_u^+)$, X-state ion $N_2^+(X^2\Sigma_g^+)$ and atomic nitrogen $N(^4S)$. The formation of these species during FLEET excitation process is still not fully understood and requires more study.

Experimental studies (Limbach and Miles 2015) using Rayleigh scattering diagnostics on FLEET emissions observed that the dissociation process was accompanied by a significant elevation in the local gas temperature and formation of acoustic waves due to the energy released. This was attributed to the fast gas heating phenomenon (Popov 2011, 2001; Peters et al. 2019) which may perturb the flow sufficiently and influence turbulence measurement using FLEET velocimetry (Limbach and Miles 2015). In the arc-jet plume, a major portion of the nitrogen molecules are vibrationally excited due to thermodynamic non-equilibrium effects in the nozzle expansion process (Hall and Treanor 1967). Since the energy demands of photodissociation or photoionization are influenced by the initial vibrational energy of the ground state (Valiev et al. 2020), the vibrationally excited nitrogen molecules in an arc-jet flow may influence the formation process of atomic nitrogen and the yield of the FLEET signal. More theoretical and experimental studies are required to evaluate this dependency. The influence of vibrationally excited nitrogen in arc-jet environments on the fast gas heating phenomenon caused by the fs-laser excitation also requires more studies.

Following the FLEET excitation process, the relaxation of the C-state nitrogen, $N_2(C^3\Pi_u)$, to its B-state, $N_2(B^3\Pi_g)$, takes place and is associated with emissions that are termed as second positive system. The emissions associated with relaxation of the B-state ion, $N_2^+(B^2\Sigma_u^+)$, to its X-state, $N_2^+(X^2\Sigma_g^+)$, are termed as the first negative system (shown in Fig. 1). Both the first negative and the second positive systems appear during the same time-frame in the spectral region, 320–410 nm. The life-times of these emissions span approximately ~ 50 ns in pure nitrogen. These emissions are short-lived and their life-times are not adequate for molecular tagging velocimetry (MTV); instead, they are utilized for thermometry to measure the gas temperature (Edwards et al. 2015). The atomic nitrogen, formed from the FLEET excitation process, goes through a three-body recombination process to produce vibrationally excited B-states, $N_2(B^3\Pi_g, v')$, mainly at the $v' = 11$ state (Michael et al. 2011). The spontaneous relaxation of the B-state nitrogen to its A-state, $N_2(A^3\Sigma_u^+, v'') \leftarrow N_2(B^3\Pi_g, v')$, results in emissions that are

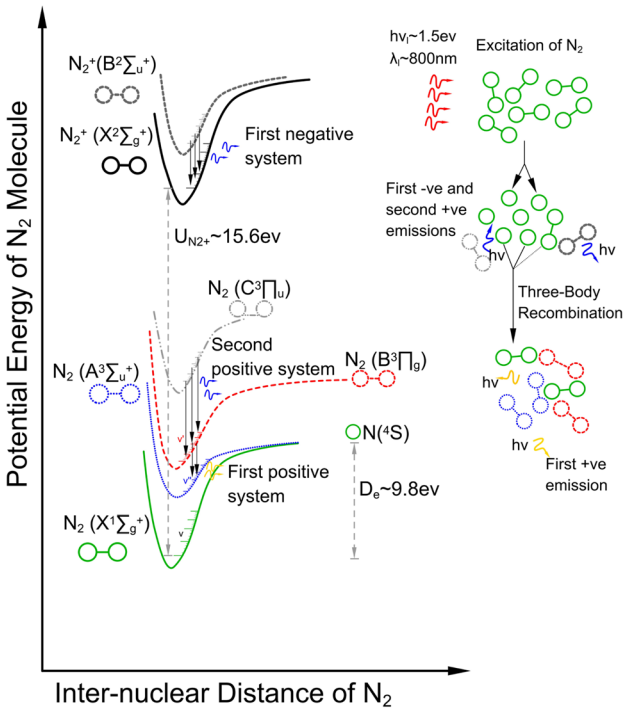

Fig. 1 Schematic representing the potential energy curves for different electronic states of N_2 and the FLEET emission processes for the first positive system

termed as the first positive system (shown in Fig. 1) and last for tens of microseconds providing ample time to detect displacement of the tagged region in high-speed flows. The B-state to A-state transition is associated with vibrational relaxation corresponding to $\Delta v = v' - v'' = 3$ and $\Delta v = 4$ bands. The spectrum of the first positive emissions lies approximately between the 500 and 900 nm wavelengths (DeLuca et al. 2014). The authors in this manuscript will refer to nitrogen first positive emissions from fs-laser excitation as simply FLEET emissions or the FLEET signal. The prior information on the FLEET emission spectrum is important for selecting optical filters to isolate the FLEET signal from the background plasma radiation in the arc-jet plume. The collisions and the relaxation process involved in the first positive system are summarized in the following reactions:

$$\mathrm{N}(^4S) + \mathrm{N}(^4S) + M \rightarrow \mathrm{N}_2(B^3\Pi_g) + M \tag{1}$$

$$\mathrm{N}_2(B^3\Pi_g, v') \rightarrow \mathrm{N}_2(A^3\Sigma_u^+, v'') + h\nu \tag{2}$$

The relaxation process of the B-state nitrogen molecule to its A-state is spontaneous, and its specific lifetime is dependent on the vibrational state (Ottinger et al. 1994; Piper et al. 1989). The primary reason for long-lived emissions in the order of $\sim 10\mu$s is attributed to the slower rate-limiting three-body collision processes described in reaction 1. The total number of three-body collisions occurring per unit time and per unit volume of the gas is proportional to $\propto n_N^2 n_{N_2} \sqrt{T_{\mathrm{trans}}}$ using the hard-sphere model (Pauly 2012). Therefore, the collision frequency has strong dependency on the number density of dissociated atomic nitrogen, n_N, the number density of diatomic nitrogen, n_{N_2}, and a weaker dependency on the local translational temperature, T_{trans}, of the gas. The recombination rate is directly dependent on the collision frequency of the gas molecules. Therefore, the intensity and the life-time of the FLEET first positive emissions are dependent on the initial number density of atomic nitrogen, n_{N_o}, (i.e., immediately after the fs-laser excitation) and the collision frequency of the molecules in the gas.

At lower number densities, like in the case of an arc-jet testing environment at sub-atmospheric conditions, the collisional rates are expected to be lower compared to atmospheric conditions. Therefore, the life-time of the FLEET signal, τ_F, is expected to be longer compared to life-time observed in atmospheric conditions. Experimental studies carried out at pressures above atmospheric conditions in a cryogenic wind tunnel (Burns et al. 2018) showed a power-law-based increase in τ_F with decrease in the density of the gas, ρ. On the other hand, the time-gated intensity of the FLEET signal, I_g, for pure nitrogen was observed to have a non-monotonic variation with the gas pressure in a laboratory environment, i.e., at room temperatures (DeLuca et al. 2014). However, the intensity studies in a cryogenic wind tunnel (Burns et al. 2018) indicated a linear dependency of the time-gated FLEET signal intensity with the gas density, $I_g \propto \rho$, in the range $\rho = 1$–7 kg/m^3. The actual temporal variation of FLEET signal intensity at different gas densities is not straightforward, and it is analyzed in detail using kinetic modeling of FLEET excitation and emission processes (Peters et al. 2019). In general, the decrease in the FLEET intensity at lower number densities can be attributed to lower collisional rates that are responsible for a slower release of photons from the first positive system. However, the signal intensity is also influenced by the initial number density of atomic nitrogen, n_{N_o}, generated by the FLEET excitation process. The population n_{N_o} decreases with the decrease in the total number density of the probed gas (Peters et al. 2019) despite an increase in dissociation fraction at lower total number densities of the gas.

Since a majority of the arc-jet testing conditions correspond to a high altitude flight environment, the static pressures of the arc-jet plume typically vary in the range of 1–100 mbar. Based on the experimental findings of FLEET intensity at low pressure in a laboratory environment by DeLuca et al. (2014), the FLEET signal is expected to be one order of magnitude lower in arc-jet flows when compared to experiments carried out in atmospheric conditions. However, as previously stated, the influence of vibrationally excited

molecules in an arc-jet flow on the intensity of FLEET signal requires experimental and theoretical investigations. Within the scope of exploring initial feasibility of FLEET in arc-jet flows, based on previous finding and considerations discussed here, a short time-gate for the intensifier coupled with large collection optics for detecting FLEET signals in the arc-jet flow play an important role for a successful velocimetry measurements. In a typical arc-jet setup, the collection optics for laser-based diagnostic experiments are usually placed far away from the hot plasma plume; therefore, a large collection optics involving either a telescopic lens or telescopic mirror will ensure a sufficient solid angle for signal detection.

2.2 FLEET velocimetry

A schematic of a typical FLEET setup is shown in Fig. 2. The focused laser forms a beam-waist with diameter, ϕ_w, and length, L_w. The tagged molecules with first positive system emissions are convected downstream along with the flow. Two separate images of the tag are captured, one at first exposure time instant, t_f, and the other at second exposure time instant $t_s = t_f + \Delta t$. In a spatio-temporally varying flow field, the tagged gas parcel convects and deforms in all the three directions as it moves through the passage of time, Δt. However, a single camera view will only detect the components of the deformation and the displacement of the tag projected onto the camera image plane. One-dimensional FLEET velocimetry assumes that the direction of the flow is known. In the schematic Fig. 2, uniform streamlines are assumed to be directed along X_{Flow} axis. Three reference frames are introduced in Fig. 2 to account for alignment difference in the direction of the flow, the orientation of the tag and the camera co-ordinate axis. The $X_{\text{Cam}} - Y_{\text{Cam}}$ are the spatial co-ordinates aligned with the camera pixel coordinates. The flow axis, X_{Flow}, is considered to be aligned with nozzle-axis that is inclined at an angle θ_N with respect to the X_{Cam}-axis. The laser beam-waist is oriented along Y_{laser}-axis at an inclination θ_L with respect to Y_{Cam}-axis.

Single point X-component of velocity measurement of a gas parcel at the nozzle centerline for FLEET velocimetry is shown in Fig. 2. The position vector of the gas parcel at the time instant t_f is $\mathbf{r}_f$ and at the time instant t_s is $\mathbf{r}_s$. Both these vectors are tracked from the $X_{\text{Cam}} - Y_{\text{Cam}}$ reference frame. The displacement vector of the tag with respect to camera reference frame during the passage of time Δt is given by $\Delta\mathbf{r} = \mathbf{r}_s - \mathbf{r}_f$. Since the flow is assumed to be one-dimensional at the nozzle center, the direction of the displacement vector, $\Delta\mathbf{r}$, is assumed to be along the nozzle axis. The Taylor series expansion for the magnitude of the displacement is then given by:

$$|\Delta\mathbf{r}| = \left|\frac{d\Delta\mathbf{r}}{dt}\right|\Delta t + \frac{1}{2!}\left|\frac{d^2\Delta\mathbf{r}}{dt^2}\right|\Delta t^2 + \frac{1}{3!}\left|\frac{d^3\Delta\mathbf{r}}{dt^3}\right|\Delta t^3 + \cdots \tag{3}$$

The first time-derivative is the velocity of the tag, $|\mathbf{V}|$, and the second time-derivative is its the acceleration, $|\mathbf{a}|$, as observed by the camera reference frame. From the kinematic perspective for the FLEET velocimetry, the appropriate choice of the delay time Δt between the two images should be chosen such that the contribution of the acceleration term to the total displacement is much less than the contribution made from the velocity term. A prior estimate on the anticipated gas velocity and acceleration can be utilized as a guide to select the delay Δt time for the experiments. In relevance to the current work, the velocity of the gas in the arc-jet plume was expected to be in the order of $|\mathbf{V}| \sim 2000$ m/s. For a contoured hypersonic nozzle, after the expansion process is completed, the acceleration of the gas is almost negligible. However, for conical nozzles in arc-jet flow the residue gas acceleration after the expansion process depends on extent to which the flow is under-expanded. A conservative estimate on the acceleration of the gas in nozzle flow can be made by taking $|\mathbf{a}| \sim |\mathbf{V}|^2/L_N$, where L_N is the length of the nozzle. Therefore, an expression to aid an appropriate selection for the delay time Δt is given by:

$$\frac{|\mathbf{a}|\Delta t^2/2}{|\mathbf{V}|/\Delta t} << 1 \;\rightarrow\; \Delta t \leq (0.01)\frac{2L_N}{|\mathbf{V}|} \tag{4}$$

The factor (0.01) limits the displacement contribution from acceleration to be 1% of the displacement contribution from the velocity. Upon substituting relevant values for the current work, the choice of the delay time is $\Delta t \leq 5\,\mu$s. For the experiments presented in this study, the delay time is chosen to be $\Delta t = 4\,\mu$s. Additionally, the expected displacement during this time duration is about $|\mathbf{V}|\Delta t \sim 8$ mm which was considered to be detectable using the camera configuration considered in this study. The expression for the velocity of the gas measured in FLEET by neglecting the acceleration and other higher-order terms is then given by:

$$|\mathbf{V}| \approx \frac{\mathbf{r}_s - \mathbf{r}_f}{\Delta t} \tag{5}$$

The double imaging process of the tag on a camera involves two separate exposure times (or gate times) with their respective delay time. The camera trigger guides the process of double imaging, and its typical plot v/s time is detailed in the schematic Fig. 3. The delay time, t_{df}, is the duration from the laser trigger to the first image trigger. The delay between the end of the first image and the start of second image is t_{ds}. Since FLEET signal decays with time, to collect sufficient photons for imaging the exposure duration (or the

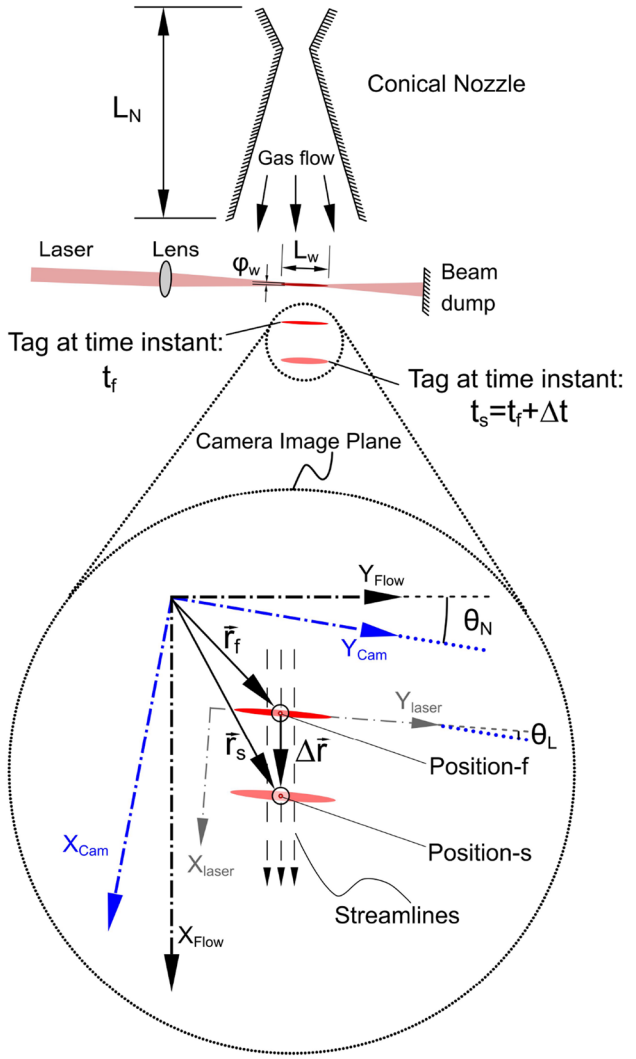

Fig. 2 Schematic of co-ordinate systems describing one-dimensional FLEET velocity measurements

gate time), t_{gs}, is usually higher than the gate time of the first image, t_{gf}. As continuous collisions between the molecules are taking place in the tag volume, the photons from FLEET emissions are released and imaged onto the camera. During this time, the tag volume is in motion with the flow as well. For simplicity in the discussion carried out here, assume that the flow is directed is along X_{Cam}. Therefore, the motion blurring effect stretches the image of the tag formed on the camera along the flow axis. The blurring effect will be more prominent in the second image with a larger time gate. The extent of motion blurring can be minimized by choosing short gated intensifier like the one utilized in this study. In our fast gate implementation, this effect is minimal (3–4 px). If the photon-flux from the tag is assumed to be constant within the gate times, then the motion blurring process is symmetrical about the center of the tag image. Additionally, diffusion process of the molecules contributes toward thickening of the tag over time. Assuming the overall thickening process is symmetrical, the appropriate time elapsed between the displacement of the imaged tag is considered as the duration between the gate-centers:

$$\Delta t = \frac{t_{gf}}{2} + t_{ds} + \frac{t_{gs}}{2} \tag{6}$$

Any deviation from the assumption of constant photon-flux during the gate-time will introduce uncertainty in the estimated time elapsed in Eq. 6. The choice of the initial delay time, t_{df}, is crucial for successful imaging of the tag at its initial position. The selection of initial time delay will depend on laser path length, L_l, from the fs-laser hardware to the probing region, the trigger wire length, L_r, from the fs-laser hardware to the camera setup, the intensifier internal delay, the distance between the tag and the camera lens, L_t, and the rate kinetics of the FLEET emissions. At low density regimes, the results of kinetic modeling (Peters et al. 2019) at room-temperatures reported initial delays of FLEET emission to last between 100 and 500 ns. The difference in the path lengths of the trigger wire and the laser pulse approximately cause a delay $\sim (L_l - L_r)/c$. The delay from the tag to the collection optics is $\sim L_t/c$. All the considerations discussed in this section played an important role in minimizing any trial-and-error of experimental parameters during an arc-jet run for successfully imaging the FLEET emissions.

3 Experimental setup

The FLEET velocimetry setup is described here for the ONR-UTA Arc-jet Wind Tunnel located at the Aerodynamics Research Center, UT Arlington. The experimental setup consists of an acquired femto-second laser system and a fast-gated intensified camera with timing circuits. The discussion of the experimental setup is briefly carried out in the following subsections. The arc-jet wind tunnel description is summarized in Sect. 3.1 and the optical systems for FLEET velocimetry in Sect. 3.3.

3.1 ONR-UTA arc-jet wind tunnel

The ONR-UTA arc-jet wind tunnel, *Leste*, at the ARC is shown in Fig. 4. The facility generates long duration high-enthalpy flow using a Thermal Dynamics F-5000 Huels type arc-heater torch that consists of a cathode barrel and an anode barrel with a gas inlet upstream of the plenum. The heater is powered by a Halmar Electronics DC electrical power supply which is rated up to 1.6MW. The power source can provide a maximum of 2000 VDC at 800 Amps during its stable operation using an input power supply

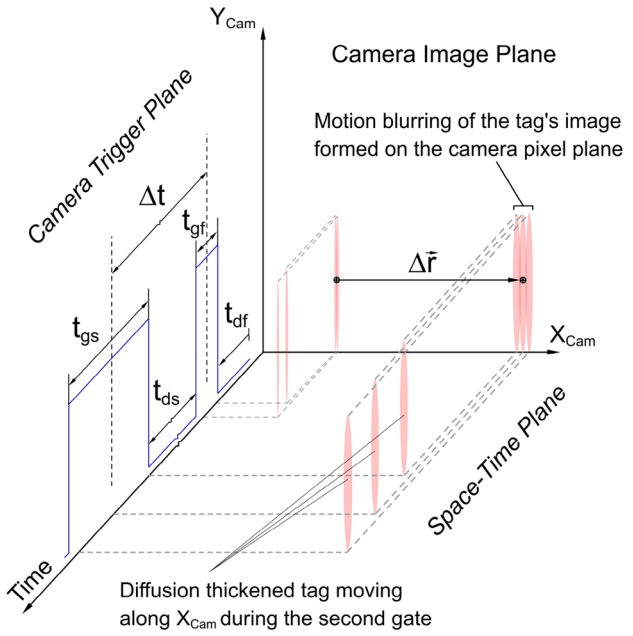

Fig. 3 Combined visualization of FLEET signal in space and time plane, camera trigger and the camera image plane

with 2400 VAC, three phase lines at 60 Hz. The input is then fed to a silicon-controlled rectifier (SCR) which provides DC power at a desired set current by the user for generating a targeted bulk enthalpy in the plenum. At high pressures, through a continuous gas flow, a direct current (DC) electric arc stretching between the cathode and the anode is stabilized by a vortex upstream of the plenum. The stable operation of the heater is carried out between 0.07 and 0.12 kg/s which can provide bulk enthalpy in the range of 2–10 MJ/kg. The high-enthalpy gas from the plenum is expanded to hypersonic speeds by an actively cooled convergent-divergent conical nozzle using deionized water as the coolant. The facility is designed to allow for the installation of interchangeable nozzle segments to produce Mach numbers between Mach 2 and 6.5 in the test section. The diameter of the Mach 6.5 nozzle is about 9 inches. The heater power, mass-flow rate, and the test section static pressure will determine the operational conditions of the arc-jet wind tunnel facility. The high-enthalpy flow is captured by an actively cooled hypersonic diffuser inlet through which the flow is compressed aerodynamically. The diffuser consists of three straight sections, followed by two diverging sections to stabilize complex shock-trains in the gas flow that is aerodynamically compressed and brought to subsonic speeds (Brune et al. 2019). The high-temperature gas is then cooled by a gas-to-water heat exchanger. The vacuum pumps pull the cooled gas at < 60 °C which is then exhausted out safely. Each vacuum pump unit consists of a Leybold DRYVAC DV650 screw pump and a RUVAC WH2500FC blower mounted in a close coupled arrangement. The facility is designed to operate with six vacuum pump units, and currently three are installed for the first phase of its operation until an envelope expansion process is carried out using all the six pumps. The test section of the facility consists of multiple modular optical ports to allow for non-intrusive diagnostics of the flow.

3.2 Arc-jet operating condition

For the arc-jet FLEET experiments discussed in this manuscript, the arc-heater was operated at 600 kW using pure nitrogen as the test gas with a corresponding mass flow rate of 0.124 kg/s and a resulting plenum pressure of 4.63 bar. The resulting bulk enthalpy, computed utilizing the energy balance method, was 2.18 MJ/kg. Using three vacuum pump units during the arc-jet run, the average test section pressure during the measurements window was measured to be 48 mbar. From the ratio of plenum to test section pressure and from the inspection of flow imaging data of the arc-jet plume, it was found that the probed region for FLEET velocimetry was located in the shock-diamond region produced from a separated flow in Mach 6.5 nozzle configuration. Since the current work focuses on the feasibility of FLEET velocimetry in arc-jet flows, the FLEET results from the shock-diamond region produced in the Mach 6.5 separated nozzle configuration are presented here. The facility has been currently configured to a Mach 4 nozzle configuration for full flow characterization, and the plume is observed to be perfectly expanded as expected.

3.3 FLEET setup

The fs-laser beam is routed through mirrors into the arc-jet test section. The beam is aligned perpendicular to the nozzle flow axis at a distance of 1 inch from the nozzle exit plane. An intensified camera with a large lens and a long-pass filter is placed on the top of the test section viewing downwards to capture the FLEET emissions. A diagram of the experimental setup is shown in Fig. 5. Inside the test section, a convex lens focused the fs-laser pulse on the centerline of the nozzle axis. The focal plane of the telescopic lens used for the intensifier and the camera was set on the nozzle central axis parallel to the X-Y plane. To measure the spectrum of the background radiation from the arc-jet plume, a convex collection lens is placed inside the test section to collect the background radiation through an optic fiber which is then routed to a spectrometer.

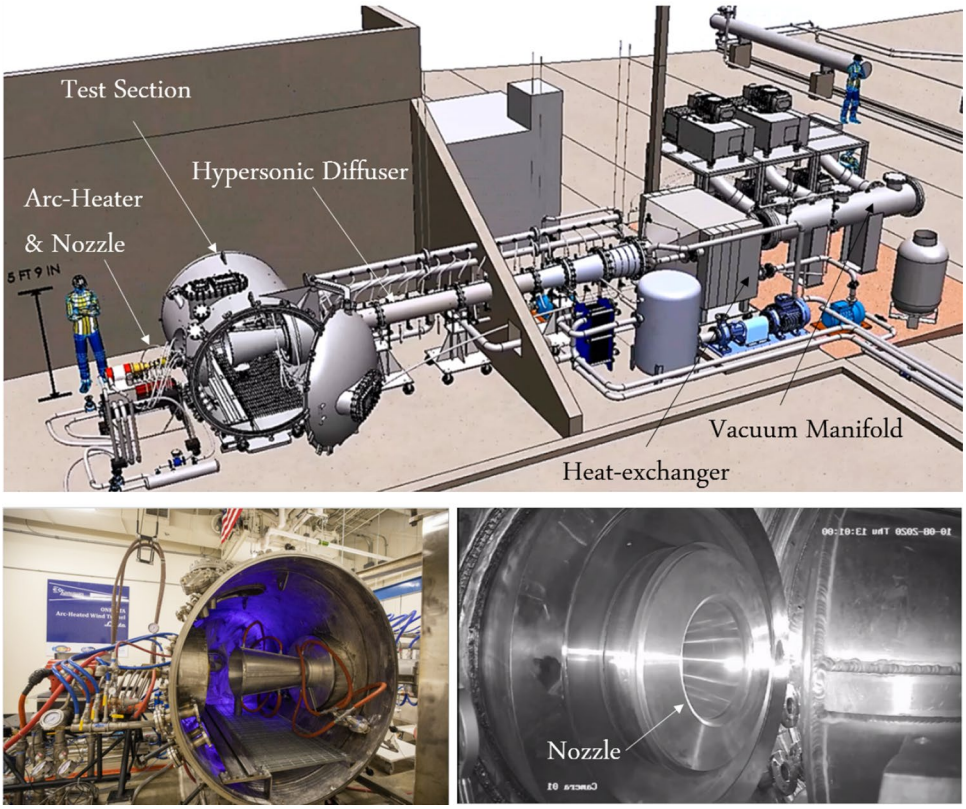

Fig. 4 ONR-UTA arc-jet wind tunnel facility, *Leste*

The fs-laser system is Spectra Physics Solstice Ace ultrafast amplifier with a pulse width of approximately $\sim 90fs$. The output beam from the fs-laser system has a nominal wavelength of 800 nm, pulse energy of 7 mJ and maximum pulse repetition of 1 kHz.

A large telescopic lens for collection optics at the top-window (Fig. 5) is located approximately at a distance of $L_t \approx 1.1$ m from the nozzle axis. The lens considered is a Nikon AF-S NIKKOR 200 mm f/2 lens. This lens has a focal length of 200 mm with a maximum and minimum aperture of f/2 to f/22. An approximate estimate on the solid angle for the collection optics in the current experimental setup is $\Omega \approx 0.0065$ Steradian. Inside the lens, an Edmunds Optics high pass filter with cut off wavelength 725 nm was selected to reduce the background radiation from the arc-jet plume. A discussion on background interference is carried out in Sect. 4.1. The large lens is mounted on a LaVision High-Speed IRO; this is a lens-coupled image intensifier. The intensified output of the high-speed IRO is coupled to a sCMOS pco.dimax S4 high-speed camera. The S4 sensor resolution is 2016×2016 pixels with a pixel size of 11×11 micrometers. The camera can operate at a maximum frame rate of 1279 frames per second. In the current experiment, the camera was operated at 200 Hz with a reduced field of view 1200×2016. This yielded a maximum recording duration of 26.5 s in the available internal memory of the camera. The entire IRO-camera setup is managed by a control box that operates on a trigger from the fs-laser system, and the arrangement is placed on an over-hanging two-axis rail-carriage mount to provide flexibility to align the camera position in the X-Y plane (shown in Fig. 5). Along the Z-axis the IRO-camera position was adjusted using an optical rail mounted on the carriage.

4 FLEET velocimetry results in arc-jet flow

Single point velocity measurement at the nozzle center is carried out using one-dimensional FLEET velocimetry. During stable operating conditions of the arc-heater, the FLEET emissions were recorded for a total of 26.5 s. A subset of the recorded FLEET images for a duration of five seconds was considered for data reduction. Some of the images were influenced by background emissions in the arc-jet plume which is discussed in Sect. 4.1. Following this discussion, the calibration process and velocity measurements are presented in Sects. 4.2 and 4.3, respectively.

4.1 Background emission spectrum and FLEET images

Arc-jet plume is typically associated with low density flow, and therefore, the FLEET signal intensity is anticipated to be less compared to atmospheric conditions (presented in

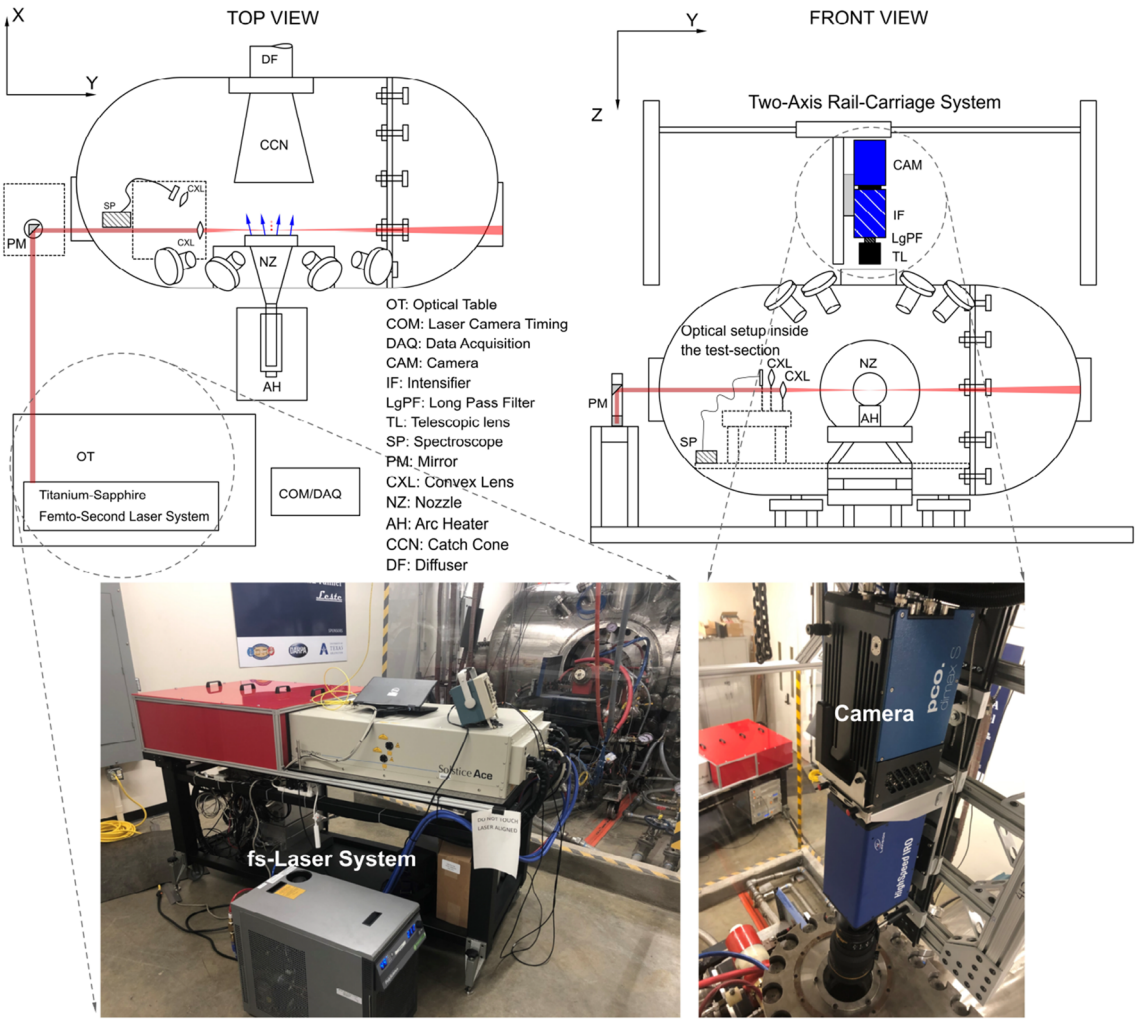

Fig. 5 FLEET setup using fs-laser and camera in the arc-jet wind tunnel, *Leste*

Sect. 2.1). To compound this challenge, the FLEET signal is immersed in a visually bright arc-jet plume with significant background radiation (shown in Fig. 6).

The radiation from the arc-jet plume is thought to arise from three sources. First, any residual plasma processes involving ions and electrons can result in emissions from the plume. However, the plasma processes causing radiation are more severe in the electric-arc formed inside the arc-heater region (Winter et al. 2012). Second, the Planck's radiation (Demtröder 2010) arises directly from the gas molecules in the arc-jet plume, and third is the scattering of the radiation from the bright electric-arc source by the gas molecules in the arc-jet plume. In a Huels type arc-heater, most of the plasma recombination processes are completed at the anode and computational studies. Takahashi et al. 2017 indicated that the electron density is two orders of magnitude lower downstream of the anode when compared to the region between the anode and the cathode. The temperature of the gas in the electric-arc region is expected to be much higher than the bulk temperature of the gas in the plenum. In the literature (Kim et al. 2005; Chang et al. 2017), typical temperatures of the electric arc in an arc-jet facility are reported in a range between 5000 and 7000 K. Application of Wien's law to the equilibrium flow in the arc-chamber results in Planck's radiation that dominates in the wavelength region 414–580 nm. The electric-arc is thought to act as a bright source of radiation in this wavelength region (shown in Fig. 6). This source radiation is then scattered by the gas molecules in the plume in all directions. In addition to this, the Planck's radiation directly from the gas molecules in the arc-jet plume is expected to peak in the near infrared region (> 1000 nm) because the gas flowing through the nozzle is expanded to cooler temperatures. However, the entire spectrum of Planck's radiation can span from visible to the near infrared regime. Recall that the first positive FLEET emissions reside between 500 and 900 nm; the main background emissions that interfere with the FLEET signal are thought to stem from the scattering of the arc radiation

by gas molecules in the arc-jet plume and a portion of the Planck's radiation spectrum that overlaps with the FLEET emissions.

In the current experiments, the spectrum of the background radiation from the arc-jet plume was measured and it is plotted in Fig. 7. The spectrum is observed to peak near ~ 550 nm. Based on these observations and analysis, a long-pass filter with a cut-off frequency of 725 nm is selected. From the measured spectrum, the filter suppressed approximately 72% of background emissions and the FLEET emissions with wavelength greater than 725 nm were recorded. A total of one thousand images were considered for the FLEET data reduction process that were collected for a duration of 5 s during the arc-jet run. Among these images, approximately 32% of them had a sufficient peak signal-to-noise ratio (PSNR) that made them eligible for the data reduction process and these details will be discussed in the subsequent paragraphs. Typical raw FLEET images which were included for data reduction and rejected for analysis are detailed in Fig. 8.

The test section contained additional monitoring cameras with infrared (IR) illumination. The reflection of this IR light from the nozzle metal flange was picked up by the sCMOS camera through the filter along with the FLEET signal as seen in Fig. 8. Care was taken during the arc-jet run to avoid overexposure of the sCMOS detector from any spurious reflections or background emissions by slowly increasing the gain of the IRO. When the sCMOS camera operates in the high-speed double exposure mode, it is observed from Fig. 8 that a ghost image from the second exposure images appears on the first exposure image. The first exposure is carried out with the delay time, $t_{df} = 345$ ns, from the laser trigger signal with exposure gate time of $t_{gf} = 10$ ns. During this initial short delay time, the displacement of the tag from the laser beam waist is very small and therefore the initial tag is undeformed. For the second exposure, the delay time was set to $t_{ds} = 3945$ ns with an exposure gate time $t_{gs} = 100$ ns. There is detectable displacement and deformation of the tag between first and the second exposure. The typical reducible raw images shown in Fig. 8 indicate the presence of spatial-temporal gradient of velocity in the arc-jet plume. During the current experiment, the intensifier was operated at 70% gain; therefore, there is potential to detect FLEET signals at lower number densities and/or with shorter second exposure gate time t_{gs}.

Each raw image in the data set is background subtracted with the average of all images recorded by the camera during the arc-jet "off" stage. The retained images are then passed through a white noise Wiener filter. The background subtracted and filtered raw images will be referred to here as processed images. These processed images contain both the FLEET signal and the residue background noise after processing. Typical processed images are shown in Fig. 9.

The distribution of signal intensity counts in the processed image will be referred to as $I(x_p, y_p)$, where x_p & y_p represent the pixel location along the X_{Cam} and Y_{Cam} axes, respectively. The signal in the neighborhood of the FLEET signal that is labeled as "noise boxes" in Fig. 9 provides information on the nature of the residue background

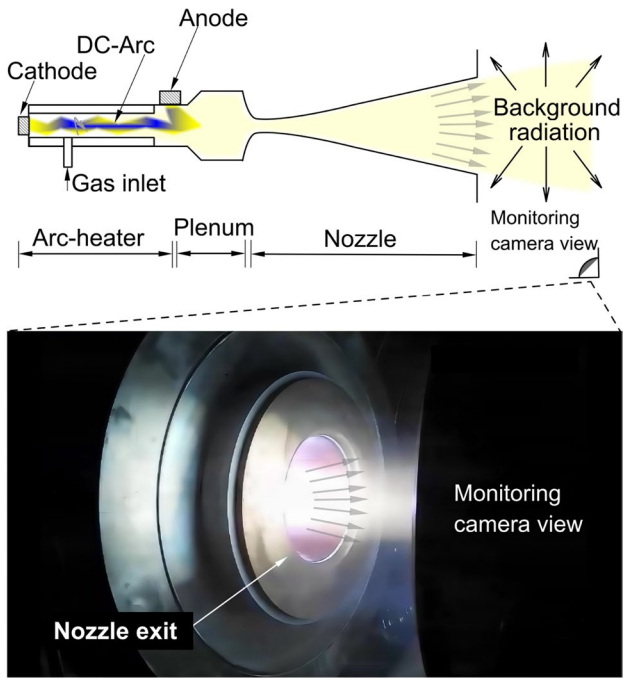

Fig. 6 Schematic of flow process in the arc-jet and a typical image of monitoring camera view during an arc-jet run

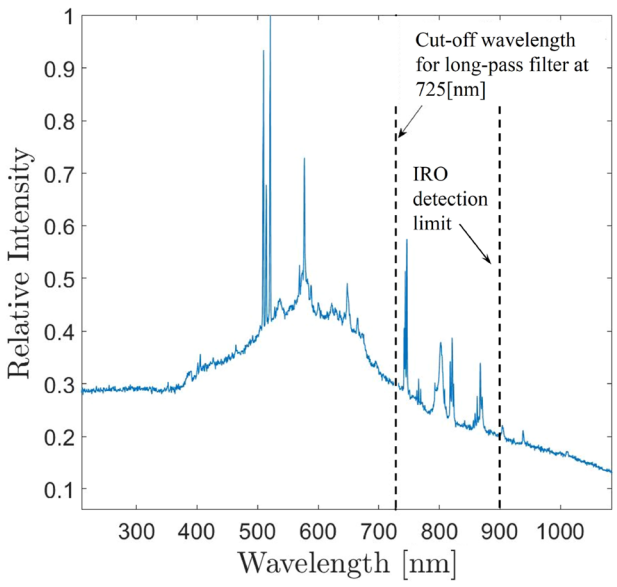

Fig. 7 Background spectrum of the arc-jet plume during FLEET experiment

signal and the noise levels affecting the FLEET signal. The camera signal distribution in each noise box as shown in Fig. 9 contains only the residue background, which will be referred to as $I_{BR}(x_p, y_p)$. The noise level, N, in a given exposure is defined as the root mean square (RMS) of the background residue signal about its mean value, $\overline{I_{BR}}$, evaluated in the noise box region, $\mathcal{R}_N$. The effect of noise, N, will be considered as the source of position uncertainty in measuring the displacement. For a given double image, the noise values in the first and second exposure will be denoted by N_f and N_s, respectively, which are evaluated in their corresponding noise boxes $\mathcal{R}_{Nf}$ and $\mathcal{R}_{Ns}$ (Fig. 9). The noise evaluated in these boxes represents the aggregate effect of background radiation, IRO noise and the camera noise. In this preliminary study, the FLEET signals for performing centerline velocimetry measurements along the nozzle axis are considered. Therefore, the signal boxes indicated by the regions, $\mathcal{R}_{If}$ and $\mathcal{R}_{Is}$ in Fig. 9, are selected in the proximity of the nozzle center and symmetrically placed about the nozzle axis to determine the centerline velocity of the gas. The height of the signal boxes was $10px$ in this study. For the first and second exposure images, the ratio of the peak signal-to-noise ratio in decibels is evaluated using $\mathrm{PSNR}_f = 20 \cdot \log_{10}\left(P_f/N_f\right)$ and $PSNR_s = 20 \cdot \log_{10}\left(P_s/N_s\right)$, respectively. Here P_f and P_s are the peak values of the FLEET signal in their corresponding signal box regions $\mathcal{R}_{If}$ and $\mathcal{R}_{Is}$, respectively. Since the noise levels, N_f and N_s, are measured about their respective mean background residue, $\overline{I_{BRf}}$ and $\overline{I_{BRs}}$, the peak values P_f and P_s in the signal boxes for each exposure

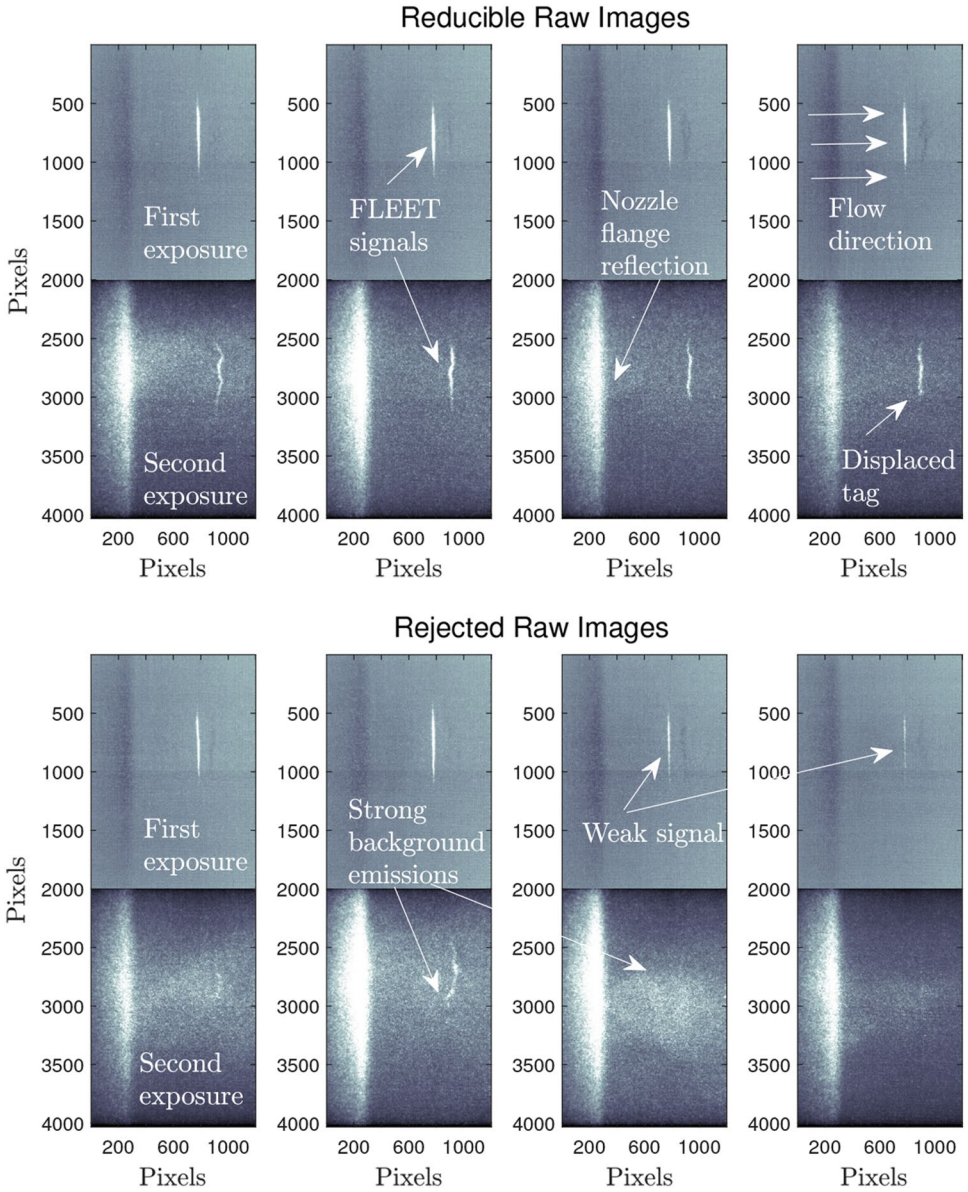

Fig. 8 Raw images of FLEET emission in double exposure mode

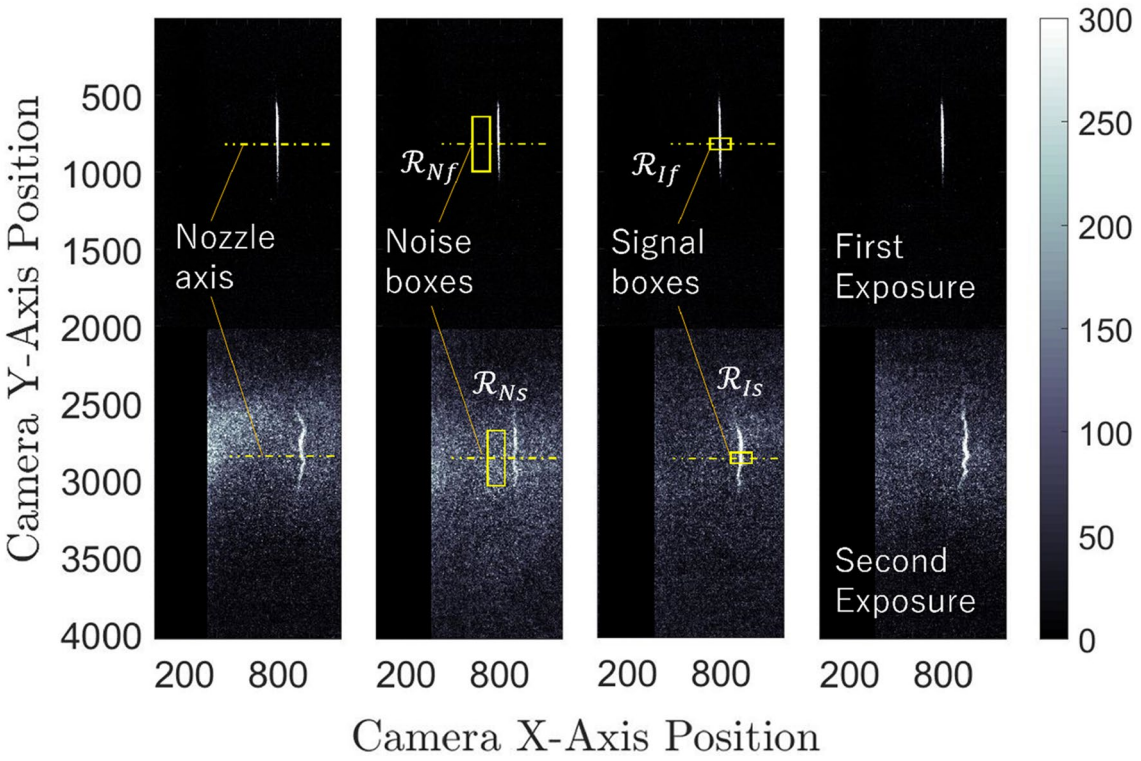

Fig. 9 Processed images of FLEET signals in double exposure mode and regions of interest

are also measured from the same reference values, $\overline{I_{BRf}}$ and $\overline{I_{BRs}}$, respectively.

The average PSNR value for all the first exposure images is 45 dB and for the second exposure images is 20 dB, i.e., a reduction in PSNR by a factor of 0.44. The reduction in PSNR of the second exposure image is primarily due to the decay of the FLEET signal with time and the noise levels in the second exposure. In the current experimental study, it was observed that the average of the FLEET gated-signal intensity in the second exposure image decreased to 67% of the signal recorded in the first exposure. This decrease in the FLEET signal was observed despite the second exposure having a higher gate time (100 ns) when compared to the first exposure image (10 ns). Since the second gate time is an order of magnitude higher than the first gate time, additional photons from the background noise are also imaged. For these reasons, the PSNR of the second exposure image is lower compared to its value in the first exposure image. The minimum PSNR in the data set that was suitable for isolating the FLEET signal for the preliminary data analysis using a gradient-based edge detection algorithm was about 11.5 dB. In the FLEET velocimetry carried out at the Sandia National Laboratories (Zhang et al. 2019), the criteria for the SNR cut off were >12 dB. This criterion was based on a limit set for displacement error less than one pixel in their study. Note that for nitrogen gas flows, it has been shown in the literature (Zhang et al. 2016; Zhang and Miles 2018) that the FLEET signal can be enhanced by seeding the flow with argon. However, the presence of diatomic oxygen in nitrogen gas flows is known to reduce the FLEET signal by more than an order of magnitude, (Michael et al. 2011, 2012). To obtain FLEET signal using air in arc-jet flows, the PSNR values need to be improved, especially for the second exposure image that is more prone to the background noise. In the FLEET work done by Zhang et al. (2019), it was suggested that the signal-to-noise ratio for the second exposure can be improved by using a smaller delay time.

4.2 Calibration and axis determination

The sCMOS camera is pointed downwards, and the telescopic lens is focused on the nozzle axis. To map the pixels to the spatial coordinates, an Edmund's calibration card with a 1 mm pattern is placed parallel to the pixel plane of the camera as shown in Fig. 10a. Since the card is placed at an arbitrary orientation in the $X_{\text{cam}} - Y_{\text{cam}}$ plane, two components of the spatial frequency are observed in the Fourier transform plane of the calibration card's image. The discrete fast Fourier transform of the calibration pattern is shown in

Fig. 10b. The location of one of the satellite maxima, $[f_x, f_y]$, in the Fourier transform plane yields the spatial frequency or the number of cycles per pixel, i.e., $f = \sqrt{f_x^2 + f_y^2}$. The spread of the maxima provides the uncertainty in the spatial frequency of the pattern. The calibration constant that maps the pixels to the spatial coordinates is then obtained by taking the inverse of the spatial frequency, $\mathcal{C} = 1/f = 18.59 \pm 0.21$px/mm.

The time-averaged image of the first exposure FLEET emissions provides a good insight into the laser orientation (shown in Fig. 10c). A best fit line along this averaged emissions indicated that the laser axis is inclined at an angle $\theta_L = 0.95$[deg] with respect to the camera Y-axis. To determine the pixel location and the orientation of the nozzle centerline, a thin rod was aligned along the nozzle axis and imaged with the sCMOS camera (shown in Fig. 10d). A best fit line along the imaged rod indicated that the nozzle centerline (or the assumed flow direction) is at an angle of 0.38 deg with respect to the X-axis of the camera. Since this is a very small angle, in the data reduction carried out in the current study the flow direction at the nozzle's center is assumed to be along the X_{Cam} axis.

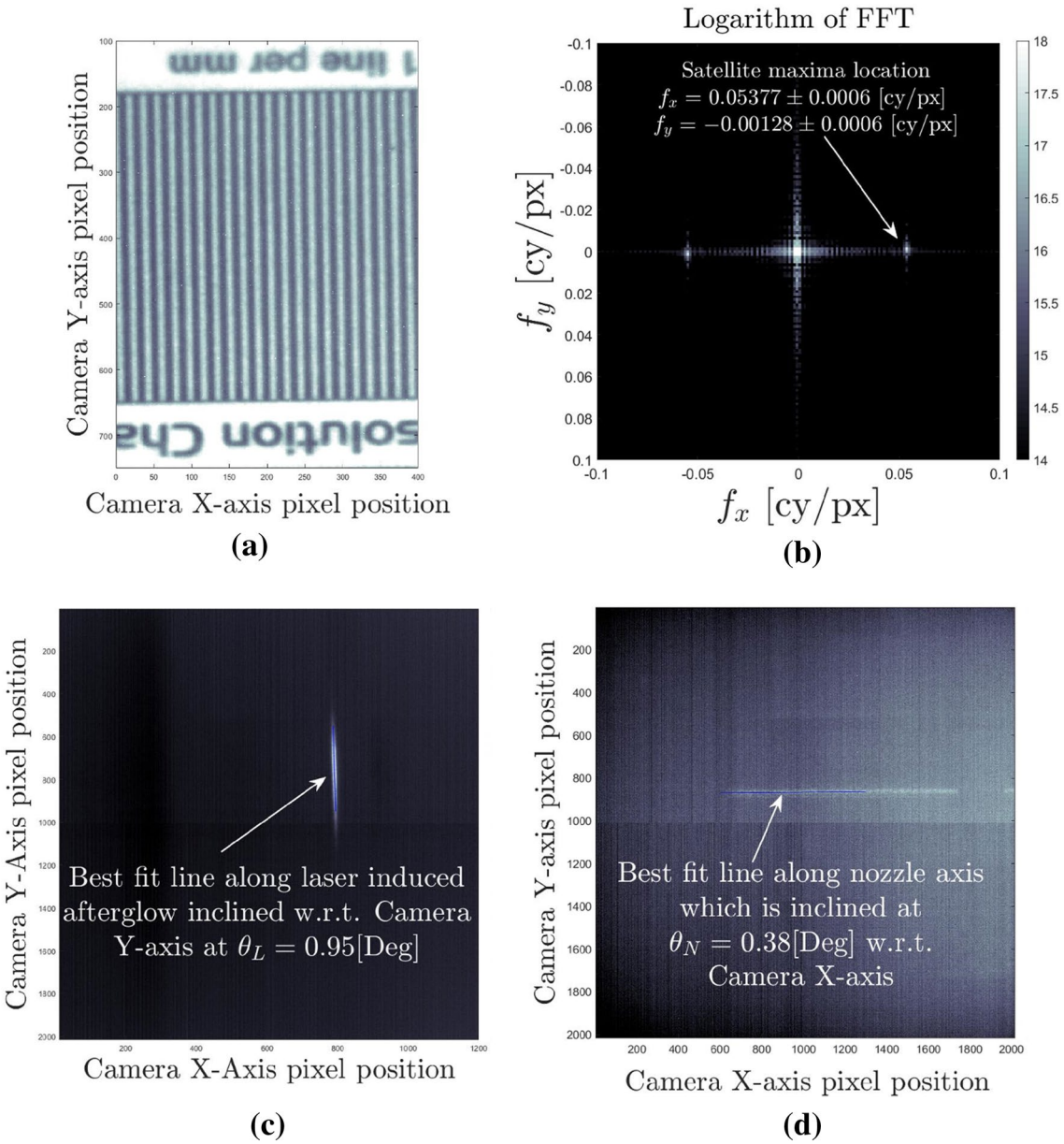

Fig. 10 **a** Image of the calibration card. **b** Discrete Fourier transform of the calibration card. **c** First exposure of the FLEET signal. **d** Image of a thin rod placed along the nozzle axis

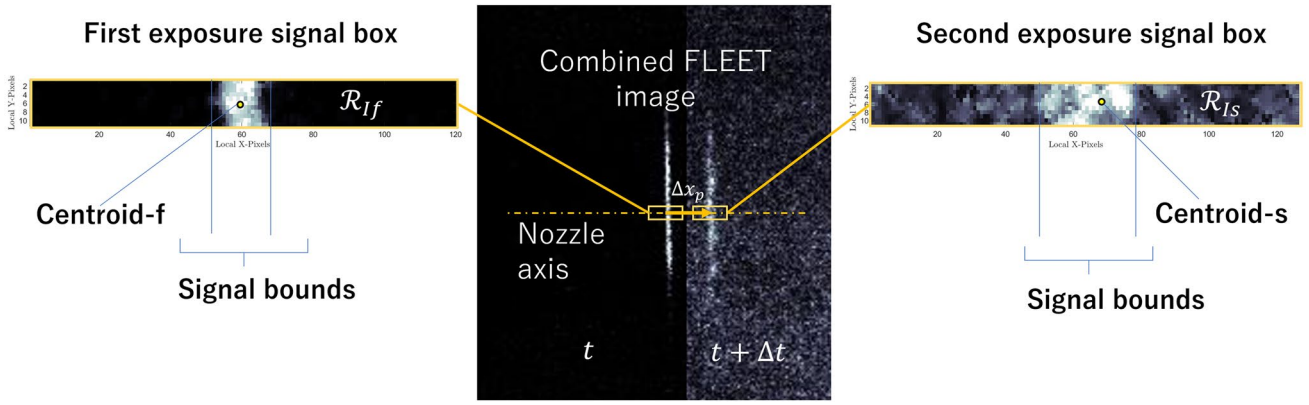

Fig. 11 Combined FLEET image and signal boxes for centerline velocity estimation

4.3 Velocimetry measurements

The scope of the current study is to explore the feasibility of quantitative FLEET measurements in arc-jet flows. For the preliminary analysis carried out here, only the X-component of velocity is measured along the nozzle axis at a single point on the nozzle center. The following analysis is described using a typical image constructed by combining the processed FLEET images for the first and second exposure shown in Fig. 11. The corresponding signal boxes for the first and second exposures are zoomed in at the left and the right of Fig. 11, respectively.

To compute the displacement for velocimetry, the centroid positions in the signal boxes, $\mathcal{R}_{If}$ and $\mathcal{R}_{Is}$, are determined using an intensity-weighted approach (Fisher et al. (2020a, 2020b)). Since the nozzle axis is closely aligned with the camera X-axis ($\theta_N = 0.38°$ deg), the displacement is computed from the difference between the X-pixel positions of centroid-f and centroid-s. The X-locations of these centroids in the pixel plane are given by:

$$x_{fp} = \left(\frac{\sum_{y_p} \sum_{x_p} I_f(x_p, y_p) x_p}{\sum_{y_p} \sum_{x_p} I_f(x_p, y_p)} \right)_{\mathcal{R}_{If}} \tag{7}$$

$$x_{sp} = \left(\frac{\sum_{y_p} \sum_{x_p} I_s(x_p, y_p) x_p}{\sum_{y_p} \sum_{x_p} I_s(x_p, y_p)} \right)_{\mathcal{R}_{Is}} . \tag{8}$$

Only the intensity of the signal encapsulated between the bounds determined from a gradient-based edge detection algorithm is isolated for centroid estimation. In the above equations to determine the centroids, $I_f(x_p, y_p)$ and $I_s(x_p, y_p)$ represent the respective isolated signal distributions in the regions $\mathcal{R}_{If}$ and $\mathcal{R}_{Is}$. Note that these isolated signals contain the sum of the signals from the FLEET emissions and the background noise. The measured displacement, $\Delta x_p = \left| x_{sp} - x_{fp} \right|$, was found to be on the order of $\sim 130px$.

For each double image, the X-component of velocity is measured along the nozzle axis at a single point on the nozzle center and it is given by:

$$V_x = \frac{\Delta x}{\Delta t} = \frac{\Delta x_p}{\mathcal{C}\Delta t} = \frac{\left| x_{sp} - x_{fp} \right|}{\mathcal{C}\Delta t} \tag{9}$$

Here, $\mathcal{C}$ is the calibration constant that maps the pixel plane to the physical plane that was determined using a discrete FFT (Sect. 4.2).

Using the error propagation rule, the uncertainty in velocity determined from each image is given by:

$$\delta V_x = \sqrt{\left(\frac{1}{\mathcal{C}^2} \frac{\Delta x_p}{\Delta t} \delta \mathcal{C} \right)^2 + \left(\frac{1}{\Delta t^2} \frac{\Delta x_p}{\mathcal{C}} \delta \Delta t \right)^2 + \left(\frac{1}{\mathcal{C}\Delta t} \delta \Delta x_p \right)^2} \tag{10}$$

As previously mentioned in Sect. 4.2, the uncertainty in the calibration constant is $\delta C = \pm 0.21$ px/mm. Assuming that the photon flux entering the camera from the FLEET emissions is constant during the short gate times, the uncertainty in the delay time, $\delta\Delta t$, is caused by the jitter between the first and second exposure delay, $\delta\Delta t = \Delta t_{\text{Jitter}} \sim \mathcal{O}(< 1\ ns)$. For flows with velocity gradients, the work done by Bathel et al. (2011) at NASA LaRC and by Zahradka et al. (2016) at AEDC estimated that a portion of the uncertainty in the axial component of velocity using tagline-based MTV techniques is due to the presence of radial/spanwise components of the velocity. The arc-jet plume is associated with a complex flow field that includes the radial and the swirl components of the velocity. As the flow is mostly axisymmetric and to perform only the centerline velocimetry, the radial and swirl components of velocity with their respective fluctuations are neglected at the nozzle center for the uncertainty analysis presented in this work. Since the current study focuses on the feasibility of FLEET velocimetry in the highly emissive arc-jet plume, only the effect of background noise on the

displacement uncertainty is considered for the preliminary analysis. In the literature (Campbell 2018; Taylor 1997), the uncertainty in an intensity-weighted centroid position due to the noise (or variance) in intensity distribution for one-dimensional analysis is specified. A simple extension of this to a two-dimensional intensity distribution is carried out by propagating errors from the noise directly to the centroid equations to determine $\delta\Delta x_p$. The velocity data along with error bars and the corresponding probability distribution are plotted in Fig. 12. In the data set chosen for this analysis, the centerline velocity mostly lied between 1700 and 1800 m/s.

The average velocity, $\langle V_x \rangle$, measured from the entire data set is 1788 m/s. The standard deviation in the velocity is estimated to be $\sigma_{V_x} = 209$ m/s which indicates the presence of velocity fluctuations in the shock-diamond region that was probed for the FLEET measurements. The total uncertainty of $\langle V_x \rangle$ is determined from the RMS of the measurement uncertainty in the data set, $\sqrt{\langle \delta V_x^2 \rangle}$, and the standard error, SE, from statistical uncertainty assuming a student-t distribution. The standard error represents the error in computing the mean value given a finite number of data points. The RMS of the measurement uncertainty in the data set is determined to be ±2.2% of the average velocity and it mainly originates from the calibration error (±1.1%) and the noise error (±1.9%). The standard error using a statistical student t-distribution is $SE = \pm 1.3\%$. Since the measurement error and standard error are independent, they are squared and summed over a square root to obtain the total uncertainty of the average velocity and it is evaluated to be ±2.6% of $\langle V_x \rangle$.

5 Conclusion

The recent development of fs-laser systems has enabled accurate measurements of the velocity of gas using the FLEET technique. Particularly, in this work the FLEET technique is applied to an arc-jet flow successfully for the first time. Given the challenges associated with background emissions, this effort has established a proof-of-concept for applying the FLEET velocimetry technique to an arc-jet flow environment. The 1.6 MW ONR-UTA arc-jet plasma wind tunnel with pure nitrogen as the test gas was the platform for the application of the FLEET velocimetry in arc-jet flows. The fs-laser dissociates diatomic nitrogen molecules in the arc-jet flow to form atomic nitrogen. These atoms recombine through a three-body collision process that results in first positive system emissions that last for tens of microseconds and thereby providing ample time for detectable displacement of the tagged molecules in the flowing gas. A camera with short time-gated recording capability with a set delay is used for sequential imaging of the tagged emissions. Two successive images recorded by the camera are utilized to calculate the spatial displacement of the tag and retrieve its velocity. The low-density arc-jet flow with significant background radiation from the plasma was thought to pose a significant challenge to the feasibility FLEET velocimetry. In the current experiments, the spectrum of the background radiation was measured and observed to peak near ~ 550 nm. This is consistent with the expected wavelengths as described due to the scattering and Planck radiation processes. From the literature, the FLEET emissions typically span between 500 and 900 nm. Based on these observations,

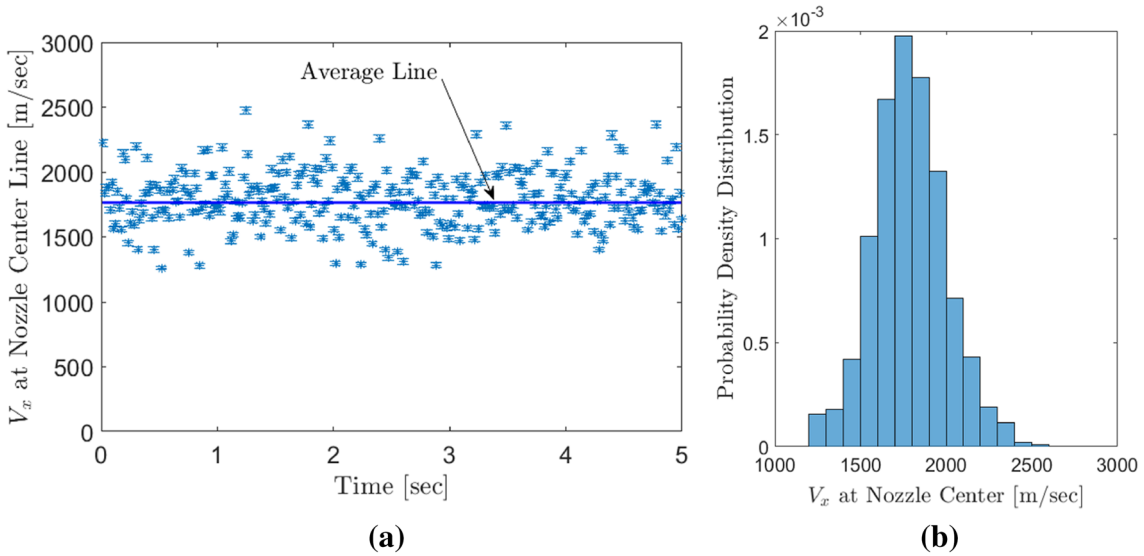

Fig. 12 **a** X-component of velocity measured at the nozzle center using FLEET v/s time. **b** Histogram representing probability density distribution of V_x measured by FLEET

a long-pass filter with a cut-off frequency of 725 nm was selected and found to approximately suppress 72% of background emissions. The FLEET emissions in the arc-jet plume were successfully imaged, and a significant spatio-temporal variation in the tag's displacement was observed. A total of one thousand images were utilized for the data reduction process. Among these images, approximately 32% of them had sufficient peak signal-to-noise ratio (PSNR) to be eligible for the data reduction process. The average PSNR value for all the first exposure images is 45 dB and for the second exposure images is 20 dB, i.e., a reduction in PSNR by a factor of 0.44. The reduction in PSNR of the second exposure image is primarily due to of the decay of the FLEET signal with time and the noise levels in the second exposure. The processed images were utilized to compute the position of the FLEET signals in the first and second exposure to provide the one-dimensional velocity along the nozzle axis. The time-averaged velocity $\langle V_x \rangle$ measured using FLEET is estimated to be 1788 m/s with a standard deviation of $\sigma_{V_x} = 209$ m/s and total uncertainty of ± 2.6 %.

References

Arepalli S (1989) Demonstration of the feasibility of laser induced fluorescence for arc jet flow diagnostics. Tech. rep., Lockheed Engineering and Management Services Co., Inc., Houston, TX (USA)

Bathel BF, Danehy PM, Inman JA, Jones SB, Ivey CB, Goyne CP (2011) Velocity profile measurements in hypersonic flows using sequentially imaged fluorescence-based molecular tagging. AIAA J 49(9):1883–1896

Beth MU, Kling M (1969) Spectroscopically measured velocity profiles of an mpd arcjet. AIAA J 7(11):2181–2182. https://doi.org/10.2514/3.5592

Brune AJ, Hosder S, Campbell D, Gulli S, Maddalena L (2019) Numerical analysis of an actively cooled low-reynolds-number hypersonic diffuser. J Thermophys Heat Transf 33(1):32–48. https://doi.org/10.2514/1.T5437

Burns RA, Peters CJ, Danehy PM (2018) Unseeded velocimetry in nitrogen for high-pressure, cryogenic wind tunnels: part i femtosecond-laser tagging. Meas Sci Technol 29(11):115302. https://doi.org/10.1088/1361-6501/aade1b

Campbell S (2018) Comparison of the generalized centroid with gaussian and quadratic peak localization methods

Danehy PM, Bathel BF, Calvert ND, Dogariu A, Miles RB (2014) Three component velocity and acceleration measurement using fleet. In: 30th AIAA aerodynamic measurement technology and ground testing conference, p 2228, https://doi.org/10.2514/6.2014-2228

DeLuca NJ, Miles RB, Kulatilaka WD, Jiang N, Gord JR (2014) Femtosecond laser electronic excitation tagging (fleet) fundamental pulse energy and spectral response. In: 30th AIAA aerodynamic measurement technology and ground testing conference, p 2227, https://doi.org/10.2514/6.2014-2227

Demtröder W (2010) Atoms, molecules and photons, vol 3. Springer

Dogariu A, Dogariu LE, Smith MS, McManamen B, Lafferty JF, Miles RB (2021) Velocity and temperature measurements in mach 18 nitrogen flow at tunnel 9. In: AIAA Scitech 2021 Forum, p 0020, https://doi.org/10.2514/6.2021-0020

Dogariu L, Dogariu A, Smith MS, Marineau EC, Miles RB (2018a) Hypersonic flow velocity measurements using fleet. In: 2018 Conference on lasers and electro-optics (CLEO), IEEE, pp 1–2

Dogariu LE, Dogariu A, Miles RB, Smith MS, Marineau EC (2018b) Non-intrusive hypersonic freestream and turbulent boundary-layer velocity measurements in aedc tunnel 9 using fleet. In: 2018 AIAA aerospace sciences meeting, p 1769, https://doi.org/10.2514/6.2018-1769

Dogariu LE, Dogariu A, Miles RB, Smith MS, Marineau EC (2019) Femtosecond laser electronic excitation tagging velocimetry in a large-scale hypersonic facility. AIAA J 57(11):4725–4737. https://doi.org/10.2514/1.J057759

Edwards MR, Dogariu A, Miles RB (2015) Simultaneous temperature and velocity measurements in air with femtosecond laser tagging. AIAA J 53(8):2280–2288. https://doi.org/10.2514/1.J053685

Fisher JM, Braun J, Meyer TR, Paniagua G (2020a) Application of femtosecond laser electronic excitation tagging (fleet) velocimetry in a bladeless turbine. Meas Sci Technol 31(6):064005

Fisher JM, Smyser ME, Slipchenko MN, Roy S, Meyer TR (2020b) Burst-mode femtosecond laser electronic excitation tagging for khz-mhz seedless velocimetry. Opt Lett 45(2):335–338

Grinstead J, Porter B, Carballo E (2011) Flow property measurements using laser-induced fluorescence in the nasa ames interaction heating facility arc jet. In: 49th AIAA aerospace sciences meeting including the new horizons forum and aerospace exposition, p 1091, https://doi.org/10.2514/6.2011-1091

Grinstead JH, Wilder MC, Porter B, Brown J, Yeung D, Battazzo S, Brubaker T (2016) Consolidated laser-induced fluorescence diagnostic systems for the nasa ames arc jet facilities. In: 32nd AIAA aerodynamic measurement technology and ground testing conference, p 4159, https://doi.org/10.2514/6.2016-4159

Hall JG, Treanor CE (1967) Nonequilibrium effects in supersonic-nozzle flows. Tech. rep, advisory group for aerospace research and development neuilly-sur-seine (France)

Heays A (2010) Photoabsorption and photodissociation in molecular nitrogen. Ph.D. thesis, Research School of Physics and Engineering, ANU College of Physical and Mathematical Sciences

Hsu PS, Jiang N, Jewell JS, Felver JJ, Borg M, Kimmel R, Roy S (2020) 100 khz pleet velocimetry in a mach-6 ludwieg tube. Opt Exp 28(15):21982–21992. https://doi.org/10.1364/OE.391302

Inman JA, Bathel BF, Johansen CT, Danehy PM, Jones SB, Gragg JG, Splinter SC (2013) Nitric-oxide planar laser-induced fluorescence measurements in the hypersonic materials environmental test system. AIAA J 51(10):2365–2379. https://doi.org/10.2514/1.J052246

Kim S, Jeffries J, Hanson R, Raiche G (2005) Measurements of gas temperature in the arc-heater of a large scale arcjet facility using tunable diode laser absorption. In: 43rd AIAA aerospace sciences meeting and exhibit, p 900, https://doi.org/10.2514/6.2005-900

Limbach C, Miles RB (2015) Characterization of dissociation and gas heating in femtosecond laser plasma with planar rayleigh scattering and rayleigh scattering polarimetry. In: 53rd AIAA aerospace sciences meeting, p 0932, https://doi.org/10.2514/6.2015-0932

Michael J, Edwards M, Dogariu A, Miles R (2012) Velocimetry by femtosecond laser electronic excitation tagging (fleet) of air and nitrogen. In: 50th AIAA aerospace sciences meeting including the new horizons forum and aerospace exposition, p 1053

Michael JB, Edwards MR, Dogariu A, Miles RB (2011) Femtosecond laser electronic excitation tagging for quantitative velocity imaging in air. Appl Opt 50(26):5158–5162. https://doi.org/10.1364/AO.50.005158

Miles R (2013) Femtosecond laser electronic excitation tagging (fleet) for imaging flow structure in unseeded hot or cold air or nitrogen. In: 51st AIAA aerospace sciences meeting including the new horizons forum and aerospace exposition, p 340, https://doi.org/10.2514/6.2013-340

Nations M, Chang LS, Jeffries JB, Hanson RK, MacDonald ME, Nawaz A, Taunk JS, Gökçen T, Raiche G (2017) Characterization of a large-scale arcjet facility using tunable diode laser absorption spectroscopy. AIAA J 55(11):3757–3766. https://doi.org/10.2514/1.J056011

Ottinger C, Smirnova L, Vilesov A (1994) Collision-induced transitions from n2 (a5+ g) to n2 (b 3π g) via the gateway mechanism. J Chem Phys 100(7):4848–4861

Pauly H (2012) Atom, molecule, and cluster beams I: basic theory,production and detection of thermal energy beams. Springer

Peters CJ, Shneider MN, Miles RB (2019) Kinetics model of femtosecond laser ionization in nitrogen and comparison to experiment. J Appl Phys 125(24):243301. https://doi.org/10.1063/1.5098306

Piper LG, Holtzclaw KW, Green BD, Blumberg WA (1989) Experimental determination of the einstein coefficients for the n2 (b-a) transition. J Chem Phys 90(10):5337–5345

Popov N (2001) Investigation of the mechanism for rapid heating of nitrogen and air in gas discharges. Plasma Phys Rep 27(10):886–896. https://doi.org/10.1134/1.1409722

Popov N (2011) Fast gas heating in a nitrogen-oxygen discharge plasma: I kinetic mechanism. J Phys D Appl Phys 44(28):285201

Reese D, Danehy PM, Jiang N, Felver J, Richardson DR, Gord JR (2018) Application of starfleet velocimetry in the nasa langley 0.3-meter transonic cryogenic tunnel. In: 2018 aerodynamic measurement technology and ground testing conference, p 2989, https://doi.org/10.2514/6.2018-2989

Scott CD (1993) Survey of measurements of flow properties in arcjets. J Thermophys Heat Transf 7(1):9–24. https://doi.org/10.2514/3.11563

Takahashi Y, Esser B, Steffens L, Gülhan A (2017) Plasma flow modeling for huels-type arc heater with turbulent diffusion. Phys Plasmas 24(12):123509. https://doi.org/10.1063/1.5008909

Taylor J (1997) Introduction to error analysis, the study of uncertainties in physical measurements

Valiev R, Berezhnoy A, Gritsenko I, Merzlikin B, Cherepanov VN, Kurten T, Wöhler C (2020) Photolysis of diatomic molecules as a source of atoms in planetary exospheres. Astron Astrophys 633:A39. https://doi.org/10.1051/0004-6361/201936230

Winter M, Prabhu D, Raiche G, Terrazas-Salinas I, Hui F (2012) Emission spectroscopic measurements with an optical probe in the nasa ames ihf arc jet facility. In: 50th AIAA aerospace sciences meeting including the new horizons forum and aerospace exposition, p 1016

Zahradka D, Parziale N, Smith M, Marineau E (2016) Krypton tagging velocimetry in a turbulent mach 2.7 boundary layer. Exp Fluids 57(5):62

Zhang Y, Miles RB (2018) Femtosecond laser tagging for velocimetry in argon and nitrogen gas mixtures. Opt Lett 43(3):551–554. https://doi.org/10.1364/OL.43.000551

Zhang Y, Calvert N, Shneider MN, Miles RB (2016) Enhancement of fleet in argon gas mixtures. In: 32nd AIAA aerodynamic measurement technology and ground testing conference, p 3249, https://doi.org/10.2514/6.2016-3249

Zhang Y, Richardson DR, Beresh SJ, Casper KM, Soehnel M, Henfling J, Spillers R (2019) Hypersonic wake measurements behind a slender cone using fleet velocimetry. In: AIAA aviation 2019 Forum, p 3381, https://doi.org/10.2514/6.2019-3381

Authors and Affiliations

Vijay Gopal[1] · Daniel Palmquist[1] · Luca Maddalena[1] · Laura E. Dogariu[2] · Arthur Dogariu[3]

✉ Vijay Gopal
vijay.gopal@mavs.uta.edu

[1] Aerodynamics Research Center, University of Texas at Arlington, Arlington, TX 76019, USA

[2] Speckodyne Corporation, Hamilton, NJ 08619, USA

[3] Princeton University, Princeton, NJ 08544, USA